Science & Technology Facilities Council

Technical Report
RAL-TR-2010-012

Calculation of background effects on the VESUVIO eV neutron spectrometer

J Mayers

March 2010

RAL Library
Science and Technology Facilities Council
Rutherford Appleton Laboratory
Harwell Science and Innovation Campus
Didcot
OX11 0QX

Tel: +44(0)1235 445384
Fax: +44(0)1235 446403
email: library@rl.ac.uk

ISSN 1358-6254

Calculation of background effects on the VESUVIO eV neutron spectrometer

J Mayers (ISIS facility, Rutherford Appleton Laboratory)

Abstract

The VESUVIO spectrometer at the ISIS pulsed neutron source measures the momentum distribution $n(\mathbf{p})$ of atoms by "neutron Compton scattering" (NCS) . Measurements of $n(\mathbf{p})$ provide a unique window on the quantum behaviour of atomic nuclei in condensed matter systems. The VESUVIO ^{6}Li doped neutron detectors at forward scattering angles were replaced in Feb 2008 by Yttrium Aluminium Perovskite doped (YAP) γ-ray detectors. These provide a much superior resolution and general performance, but suffer from a sample dependent gamma background. This report details how this background is calculated and data corrected. The report also indicates how this background can be reduced.

1. Introduction

The VESUVIO spectrometer at the ISIS pulsed neutron source measures the momentum distribution $n(\mathbf{p})$ of atoms by "neutron Compton scattering" (NCS) [1]. Measurements of $n(\mathbf{p})$ provide a unique window on the quantum behaviour of atomic nuclei in condensed matter systems. NCS is of particular value for studying the large number of important systems containing protons - for example, water, biological molecules, hydrogen storage materials, protons conductors, metal hydrides etc. Examples of recent measurements in various systems are given in references [2,3,4,5,6,7,8].

Interpretation of VESUVIO data relies upon the fact that for scattering with sufficiently high momentum and energy transfers, the impulse approximation (IA) is accurate [9]. The IA implies that the neutron scatters from a single atom, with conservation of the total kinetic energy and momentum of the neutron plus atom. Hence the measured energy and momentum change of the neutron is related in a simple way to the momentum distribution of the atoms. Details of the technique and the data analysis used are given in references [1] and [10].

Measurements of proton momentum distributions require much higher energy and wave vector transfers than those accessed by other neutron scattering techniques. Typically the energy transfer is $1 < \omega < 50$ eV and the wave vector transfer $40 < q < 150$ Å^{-1}. NCS is possible only at pulsed neutron sources, which allow the use of time of flight techniques [11] for accurate inelastic neutron scattering measurements at eV energies.

Time of flight techniques require that the energy of either the incident or scattered neutron is well defined. On VESUVIO this is accomplished by use of the neutron absorption resonance which occurs in gold at 4.9 eV [12]. This defines the final energy of the neutron as 4.9 $\pm$ ~0.14 eV. The long (almost Lorentzian) wings of the gold absorption cross-section have previously allowed only modest resolution in atomic momentum space. However a new technique has recently been adopted, which significantly improves the energy resolution function of VESUVIO.

The VESUVIO ^{6}Li doped neutron detectors at forward scattering angles have been replaced by Yttrium Aluminium Perovskite doped (YAP) γ-ray detectors [13,14,15]. Although these do not detect neutrons directly, they are made to function both as neutron detectors and energy selectors by placing a gold foil on the YAP detector surface [16]. When the foil absorbs neutrons in the 4.9 eV resonance it emits a γ-ray cascade which can be detected, thereby determining both the time of flight and the final energy of the neutron.

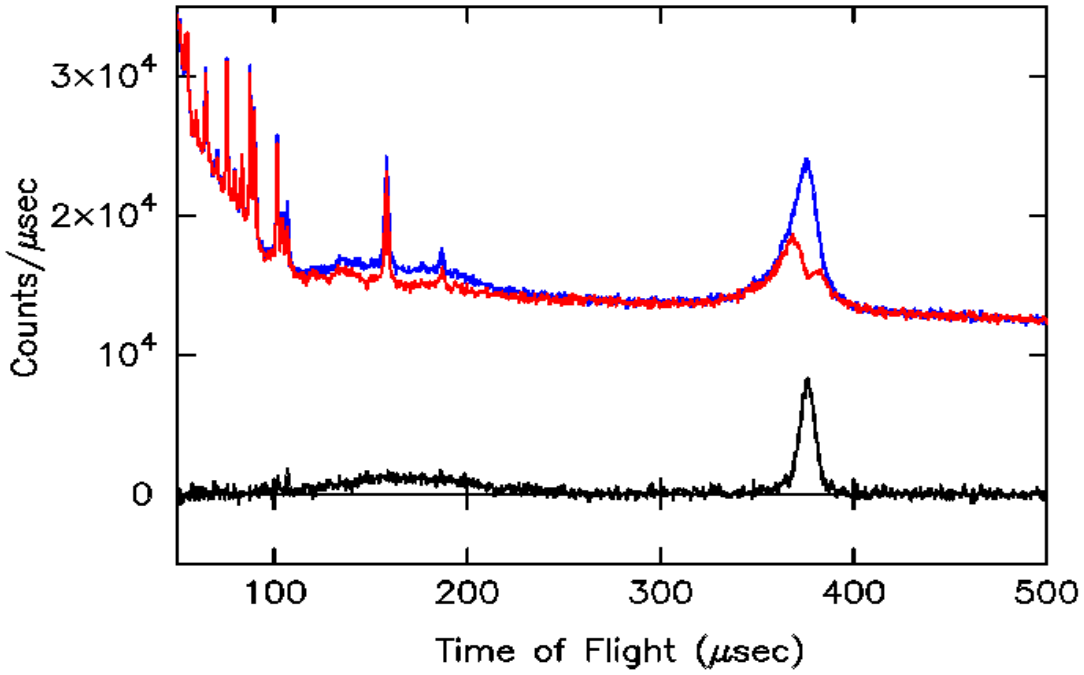

Figure1. Data taken from a sample composed of sheets of polythene (CH_2) and lead by a single YAP detector at an angle of 67º. The "foil out" data is in blue. The "foil in" data is in red. The difference "foil out"-"foil in" is shown as the black line. The scattering angle was 66º. The total count time was 5600 micro-amp-hours. The sample scattered 15% of the incident beam.

The blue line in Figure 1 shows time of flight data obtained in a single YAP detector at a scattering angle of 66º, from a sample composed of sheets of lead and polythene (CH_2). The peak at ~ 380 μsec is due to scattering from lead and carbon, that at ~170 μsec from hydrogen. It can be seen that the γ-ray signal from the foil sits on a large background. This seems to be mainly due to γ-ray rays produced when neutrons scattered by the sample are absorbed by the surrounding boron shielding.

By use of a secondary foil which can be placed in two positions the energy resolution can be much improved and the background almost eliminated. This "foil cycling" method [17] is illustrated in Figure 2.

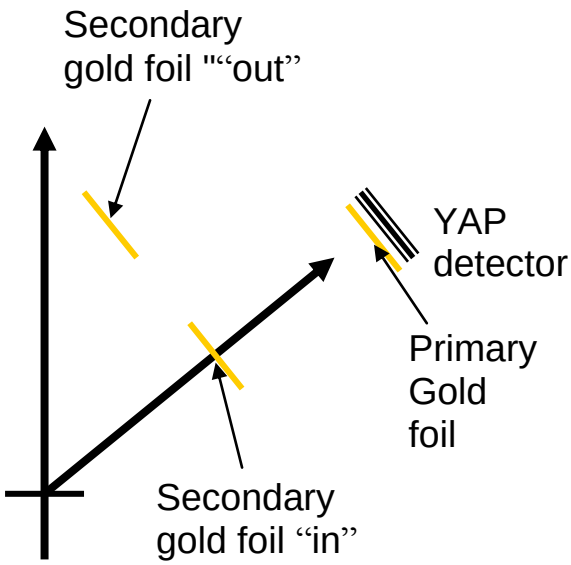

Figure 2. Illustrates the foil cycling method used on VESUVIO. There is a primary gold foil fixed on the surface of the YAP detector and a moveable secondary gold foil of identical thickness. The secondary foils are “cycled” that is moved many times between the two positions within a data collection period. The cycling removes drifts in detector efficiency with time, due for example to ambient temperature changes.

In the "foil out" measurement (shown as the blue line in Figure 1), the scattered neutrons do not have to pass through the secondary foil to reach the primary foil. The "foil out" counts are

$$C_{out}(E_0, E_1, \theta_d) = C(E_0, E_1, \theta_d) A(E_1) \eta + B_{out}(E_0, E_1, \theta_d) \qquad (1.1)$$

E_0 is the energy of the neutron incident on the sample, E_1 is the energy of the scattered neutron absorbed by the foil and θ is the scattering angle. $C(E_0, E_1, \theta_d)$ is the rate at which scattered neutrons are incident on the primary foil. $C(E_0, E_1, \theta_d)$ depends on the incident neutron spectrum and the scattering properties of the sample and can be determined from the data as described in Appendix 1. $A(E_1)$ is the probability that a neutron of energy E_1 is absorbed in the primary foil. η is the probability that the consequent γ-ray cascade is registered by the YAP detector. B_{out} is the γ background with the secondary foil "out".

In the “foil in” measurement the secondary foil is moved so that neutrons have to pass through it to reach the primary foil. Currently the secondary foil has the same thickness as the primary foil. Hence the counts from the primary foil are reduced by the factor $1 - A(E_1)$.

$$C_{in}(E_0, E_1, \theta) = C(E_0, E_1, \theta)\left[1 - A(E_1)\right] A(E_1) \eta + B_{in}(E_0, E_1, \theta) \qquad (1.2)$$

A typical “foil in” spectrum is shown in Figure 1 as the red line. The VESUVIO "raw" data is the difference between these two counts.

$$C_{out} - C_{in} = C \eta A^2 + (B_{out} - B_{in}) \qquad (1.3)$$

This is illustrated as the black line in Figure 1. Clearly most of the γ-ray background is removed by this differencing technique.

It can be seen from eqs (1.1) and (1.3) that the (almost) Lorentzian energy dependence of $A(E_1)$ in the "foil out" measurement becomes a Lorenzian-squared dependence in the difference measurement. Thus not only does the foil cycling method remove most of the gamma background but it also greatly improves the resolution function. This is illustrated in Figure 3, which shows lead data collected with the old ^{6}Li doped neutron detectors [18] and the new YAP system as a function of energy transfer, $(E_0 - E_1)$. The energy resolution function with the ^{6}Li detectors is almost Lorentzian with a FWHM of ~0.35 eV. The energy resolution with the YAP detectors is almost Gaussian with a FWHM of ~0.2 eV [19].

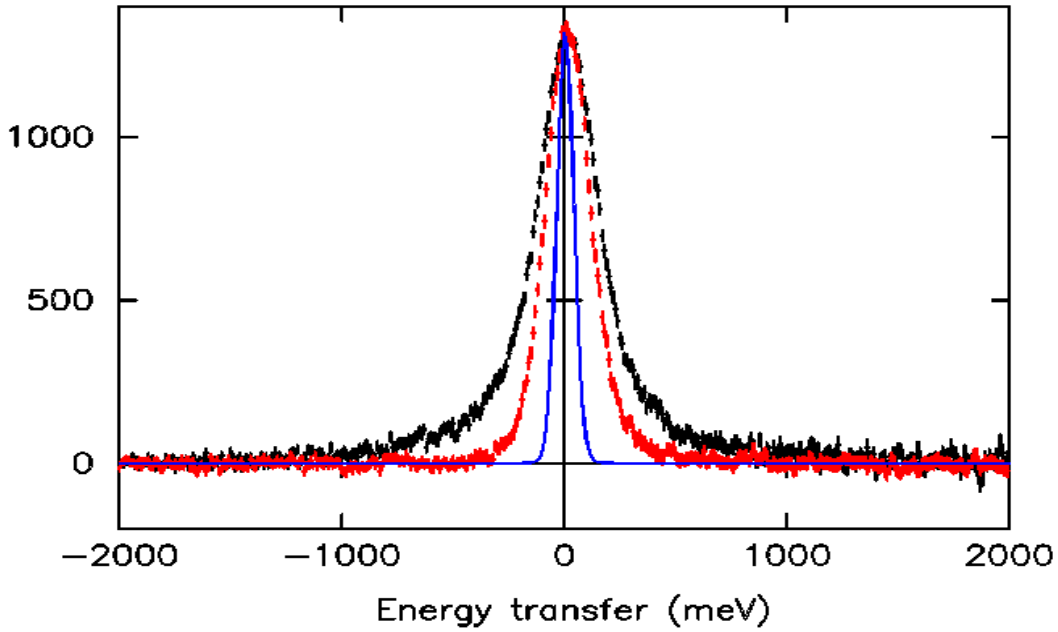

Figure 3. Shows VESUVIO data collected on a Pb sample with the old detector ^{6}Li doped neutron detectors (black) and the new YAP detector system (red) as a function of energy transfer $(E_0 - E_1)$. The intrinsic width due to the lead momentum distribution is shown as the blue line.

The "residual background" $(B_{out} - B_{in})$ in eq (1.3) is primarily due to gamma rays emitted by the secondary foils. When the secondary foil absorbs neutrons it also emits γ-rays, which can be registered by the YAP detectors. The residual background is non-zero because the intensity of these is different in the two positions occupied by the secondary foil. With the current arrangement of foils and detectors on VESUVIO the residual background is at the ~5% level compared to the signal. The main purpose of this report is to show how this residual background can be calculated and data corrected.

Section 2 describes how the residual background can be determined from the data, given the instrument geometry. Section 3 presents results of calculation for two different secondary foil geometries. Section 4 compares measured data with calculation. Section 5 describes how

data can be corrected for γ background. Section 6 discusses how the results of data analysis are affected by the background. Section 7 discusses how the residual background can be minimised. Appendix 1 contains relevant details of the data analysis on VESUVIO. Appendix 2 contains calculations of the efficiency with which γ-rays emitted by the primary foil are registered by the YAP detectors. Appendix 3 gives details of the computer programs used in the numerical calculations.

2. Calculation of Residual Background

2a Calculation of counts from the primary foil

The geometry of the calculation is illustrated in Figure 4. We consider a plane element of the primary foil, of area dA_d with its centre at distance r_d from the sample centre and at a scattering angle θ_d.

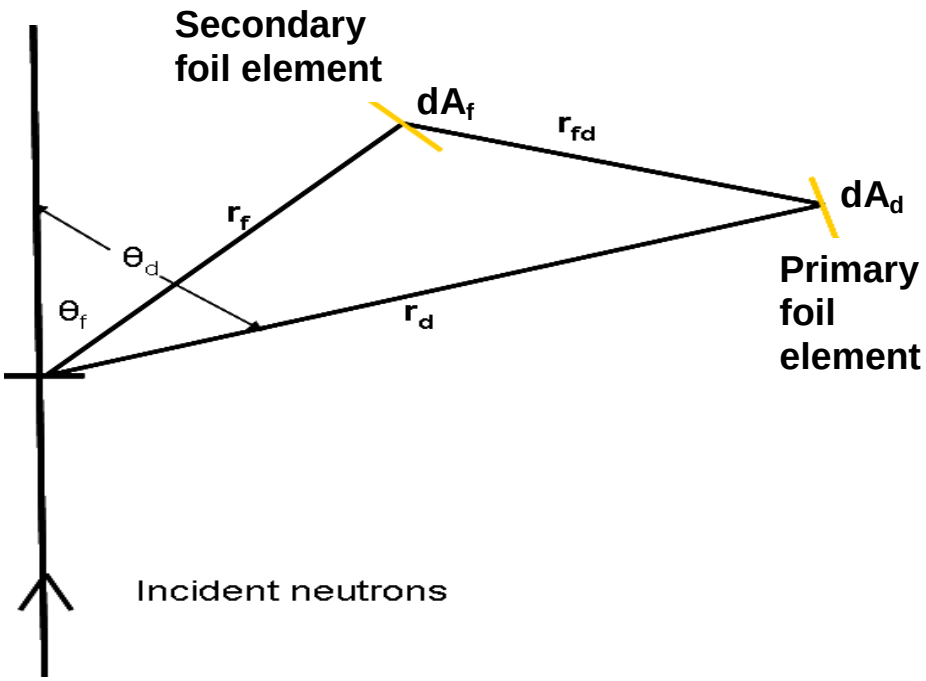

Figure 4 . Illustrates the geometry of the calculation of the counts from primary and secondary foils.

The detectors are arranged with their planes perpendicular to the line joining the sample centre and the detector centre. Hence to a very good approximation the solid angle subtended at the sample centre by any primary foil element is

$$d\Omega_d = \frac{dA_d}{r_d^2} \qquad (2.1)$$

In the "foil out" measurement the rate at which neutrons of energy E_1 are incident on the primary foil element is

$$dR_p(E_0, E_1, \theta_d) = C(E_0, E_1, \theta_d) d\Omega_d \qquad (2.2)$$

where $C(E_0, E_1, \theta_d)$ is defined in section 1 and Appendix 1. The probability $P_d(E_1)$ that a neutron of energy E_1 incident on the primary foil element is registered by the YAP detector is

$$P_d(E_1) = A(E_1)\eta \qquad (2.3)$$

$A(E_1)$ is the probability that the neutron is absorbed and η is the probability that the consequent γ-ray cascade emitted by the foil is registered by the detector. η ~0.1 [20] is a constant which depends upon the nature of the γ-ray cascade and the efficiency of the detector. It is shown in Appendix 2 that

$$\eta = \tfrac{1}{2}\alpha\mu d \qquad (2.4)$$

Where μ is the average attenuation length of emitted γ-rays in the scintillator glass and d is the glass thickness. The factor one half arises because half the gamma rays are emitted in the opposite direction to the detector. α is a constant ~1, which can be determined by fitting to calibration data (see section 5)

It follows from eqs (2.1) - (2.4) that the count rate dP_{out} from the primary foil element is

$$dP_{out}(E_0, E_1, \theta_d) = dR_p P_d(E_1) = C(E_0, E_1, \theta_d)\frac{dA_d}{r_d^2} A(E_1)\tfrac{1}{2}\alpha\mu d \qquad (2.5)$$

With the secondary foil "in" the counts from the primary foil are reduced by the factor $[1 - A(E_1)]$

$$dP_{in}(E_0, E_1, \theta_d) = [1 - A(E_1)]dP_{out}(E_0, E_1, \theta_d) \qquad (2.6)$$

Since the γ-rays are emitted effectively instantaneously on the time scales measured and take negligible time to travel to the detector, these γ-rays are detected at time t_p, determined by the distance r_d of the foil from the sample.

$$t_p = \frac{L_0}{v_0} + \frac{r_d}{v_1} \qquad (2.7)$$

v_0 is the speed of the incident neutron, v_1 that of the scattered neutron and L_0 is the flight path from moderator to sample.

2b Calculation of counts from the secondary foils

We consider an element of the secondary foil of area dA_f, with its centre at distance r_f from the sample and at a scattering angle θ_f (see Figure 4). The solid angle subtended by the element at the sample is (cf. eq 2.1)

$$d\Omega_f = \frac{\hat{\mathbf{r}}_f . \hat{\mathbf{n}}_f dA_f}{r_f^2} \qquad (2.8)$$

$\hat{\mathbf{r}}_f$ is the unit vector along the direction from the centre of the sample to the centre of the secondary foil element. $\hat{\mathbf{n}}_f$ is the unit vector perpendicular to the element. The probability that a neutron of energy E_1 incident on the element is absorbed is (see Figure 4b)

$$P_f(E_1) = 1 - \exp\left[-Nt\sigma(E_1)/(\hat{\mathbf{r}}_f.\hat{\mathbf{n}}_f)\right] \qquad (2.8a)$$

The gold absorption cross-section $\sigma(E_1)$ is calculated from tabulated resonance parameters [21], using the algorithm given in reference [12]. Nt is the number of gold atoms/unit area of foil and is determined by weighing the foil.

The rate at which neutrons of energy E_1 are absorbed by the secondary foil element is (cf. eq 2.2)

$$dR_f = P_f(E_1)C(E_0, E_1, \theta_f)d\Omega_f \qquad (2.9)$$

After absorption of a neutron, the secondary foil element emits γ-ray rays isotropically. The probability that one of these passes through a YAP detector element of area dA_d is therefore[i]

$$P_{fd} = \frac{d\Omega_f}{4\pi} = \frac{1}{4\pi}\frac{\hat{\mathbf{r}}_{fd}.\hat{\mathbf{n}}_d dA_d}{r_{fd}^2} \qquad (2.10)$$

$\hat{\mathbf{r}}_{fd}$ is the unit vector along the line from the secondary to primary foil element, $\hat{\mathbf{n}}_d$ is the unit vector perpendicular to the element (see Figure 4b) and r_{fd} is the distance between the two elements (see Figure 4a). The probability that the γ-ray is absorbed by the YAP detector is (see Figure 4b)

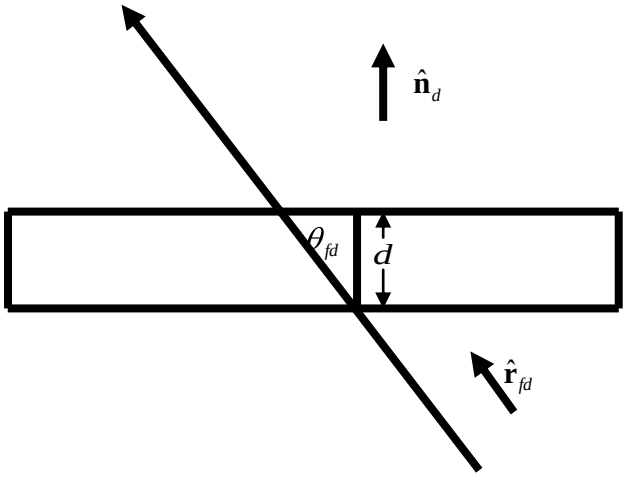

Figure 4b. Illustrates the path length of the γ-rays in the YAP scintillator glass.

$$P_{ab} = 1 - \exp(-\mu d/\cos\theta_{fd}) = 1 - \exp(-\mu d/\hat{\mathbf{r}}_{fd}.\hat{\mathbf{n}}_d) \approx \mu d/\hat{\mathbf{r}}_{fd}.\hat{\mathbf{n}}_d \qquad (2.11)$$

[i] Since the primary foil is the same area as the detector and the detector is thin, the same symbols can be used for primary foil element and detector element.

It follows from eqs (2.9)-(2.11) that the rate at which γ-rays from the secondary foil element are registered by the detectors is

$$dS(t_f) = dR_f P_{fd} P_{ab} = P_f(E_1) C(E_0, E_1, \theta_f) \frac{\hat{\mathbf{r}}_f . \hat{\mathbf{n}}_f dA_f}{r_f^2} \frac{1}{4\pi} \frac{dA_d}{r_{fd}^2} \mu d \quad (2.12)$$

These are detected at a time t_f, determined by replacing r_d by r_f in eq (2.3).

Residual background

The total counts $P_{out}(t_p)$, from the primary foil, with the secondary foils in the "out" position, is found by numerically integrating equation (2.6) over the primary foil area A_d. Similarly $P_{in}(t_p)$ is found by numerically integrating equation (2.7). The total counts $S_{out}(t_f)$ and $S_{in}(t_f)$ from the secondary foils in the two positions are found by integrating equation (2.12) over both A_d and the areas A_f of all secondary foils. It is assumed that γ-ray background not due to the secondary foils is the same in the two secondary foil positions. Hence it follows that

$$C_{out} - C_{in} = (P_{out} - P_{in}) + (S_{out} - S_{in}) \quad (2.13)$$

The signal to background ratio is defined as

$$S = (P_{out} - P_{in}) / (S_{out} - S_{in}) \quad (2.14)$$

3. Results of calculations.

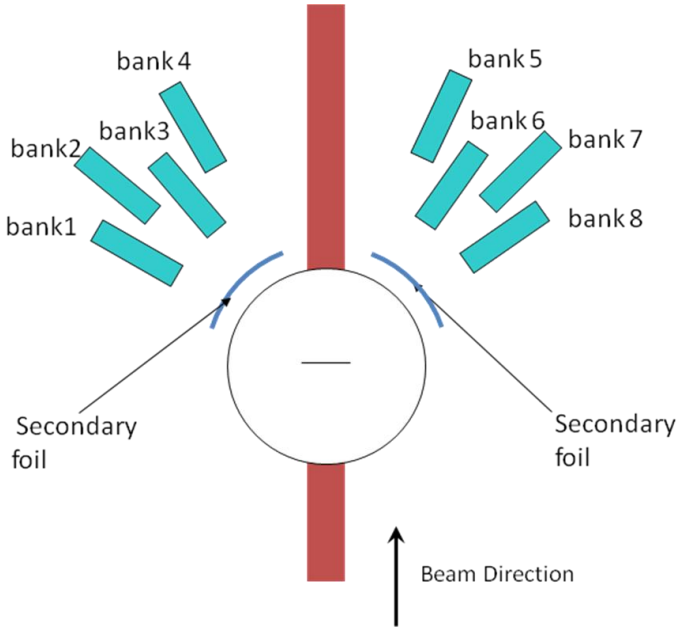

Figure 5. Illustrates YAP detector configuration on VESUVIO, looking from above. Secondary foil geometry A is also illustrated.

The geometry of the YAP detectors on VESUVIO is illustrated in Figure 5. There are 64 detectors arranged in almost vertical columns of 8 detectors, with 4 above and 4 below the "sample plane" - that is the horizontal plane passing through the sample centre. Each detector element is 8cm in height, 2.5 cm in width and of thickness ~6mm. The closest detectors are ~55 cm from the sample, while the furthest detectors are ~76 cm from the sample. The arrangement of detectors looking from moderator to sample is listed in table 1.

	Bank 1	Bank 2	Bank 3	Bank 4		Bank 5	Bank 6	Bank 7	Bank 8
h (cm)	ϕ =56º	ϕ =52º	ϕ =42º	ϕ =32º		ϕ =38º	ϕ =47º	ϕ =57º	ϕ =67º
	r_d=56	r_d =76	r_d =56	r_d =76		r_d =76	r_d =56	r_d =76	r_d =56
+37	1	9	17	25		33	41	49	57
+29	2	10	18	26		34	42	50	58
+22	3	11	19	27		35	43	51	59
+10	4	12	20	28		36	44	52	60
0									
-10	8	16	24	32		40	48	56	64
-22	7	15	23	31		39	47	55	63
-29	6	14	22	30		38	46	54	62
-37	5	13	21	29		37	45	53	61

Table 1. Positions of the 64 YAP detectors looking from source to sample. ϕ is the approximate scattering angle in the sample plane. h is the approximate height of the detector above (+) or below (-) the sample plane in cm. r_d is the approximate distance in cm of the detectors from the sample.

3a Secondary foil Geometry A

Secondary foil geometry A consisted of two foils each 20 x 20 cm and fixed on a cylindrical holder at a distance of 22.5 cm from the sample centre. In the "up" position the centres of the two secondary foils were 10 cm above the sample plane. In the "down" position they were 10 cm below this plane. Detectors above the sample plane are "foil in" in the "up" position and "foil" out in the "down" position. The reverse is true for detectors below the sample plane.

Figure 6 shows the results of calculations of the intensities from primary and secondary foils for a Pb sample. The signal from the primary foil $\left(P_{out} - P_{in}\right)$ is shown as black. The counts S_{out} from the secondary foils in the out position are shown as blue. The counts S_{in} from the secondary foils in the in position are shown as red. The calculated data with the residual background, given by eq. (2.13) is shown as the green line. The same colour coding is used for all such calculations throughout the paper.

Note that the peak from the secondary foils is centred at a different position to that from the primary foil. This is due to the different distances travelled by the neutrons to the primary and secondary foils. The primary foil is at ~55 cm and the secondary foil at 22.5 cm. Hence the time of detection of neutrons of energy 4908 ev, (with velocity 3.0640 x10^6 cm/sec) is shifted by ~ 11 μsec.

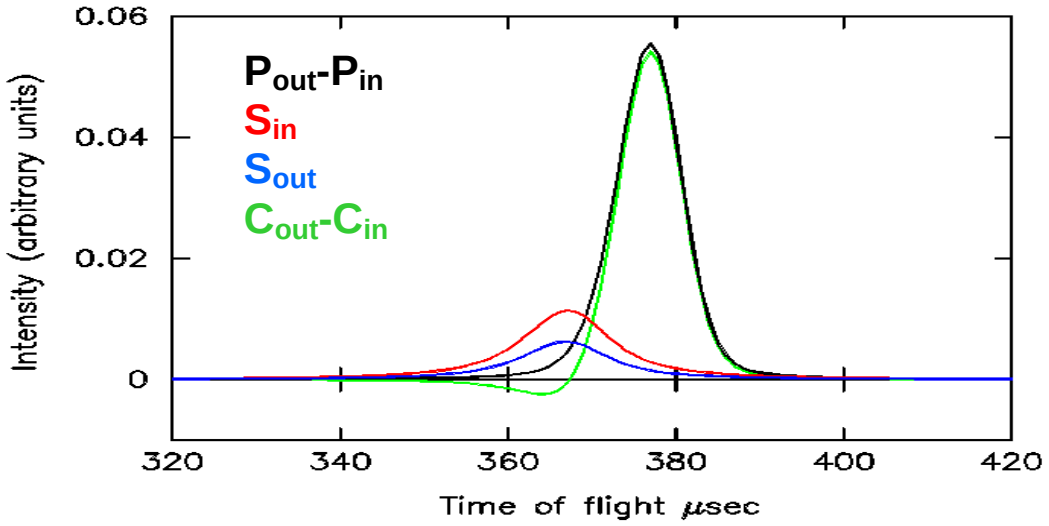

Figure 6. Calculation of scattering from lead into detector 1 in table 1, (θ=66.6º and L_1=55cm, top detector) with foil geometry A.

Figure 7 shows the same calculation for a sample of ZrH_2 at two different angles and detector distances. It can be seen that the residual background from hydrogenous samples is a worse problem for the detector in the lower plot. This is partly because the detector is closer to the sample (see section 6). It is aggravated by the fact it is also at a larger scattering angle. The hydrogen cross-section decreases strongly with angle. Hence $\left(P_{out} - P_{in}\right)$ is smallest at high scattering angles θ, whereas S_{out} and S_{in} have a much weaker dependence on scattering angle.

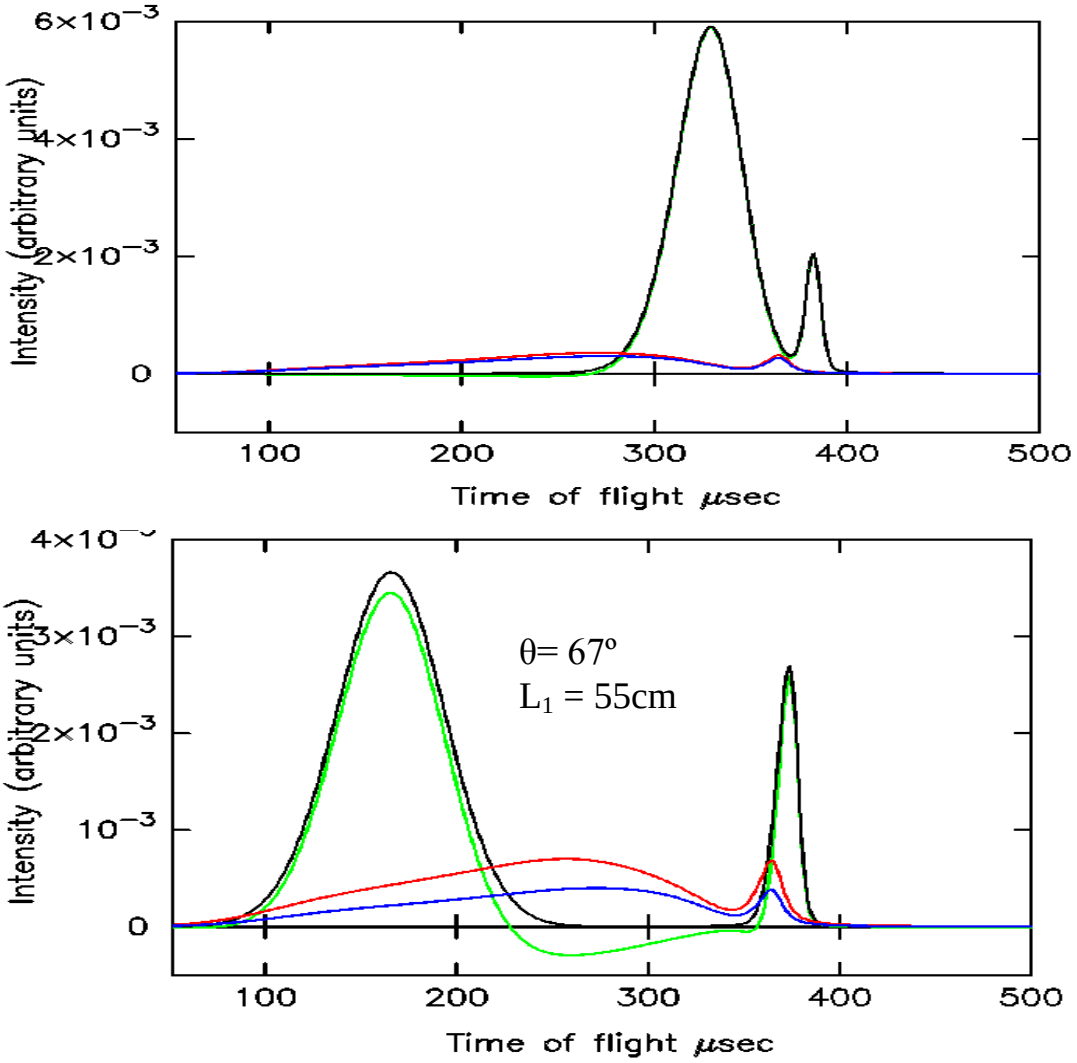

3b Secondary Foil Geometry B

The detector geometry was unaltered, but there were 4 secondary foils, two on each side of the beam line as illustrated in Figure 11. Each foil was 40 cm in length (along the vertical direction) and 4 cm wide.

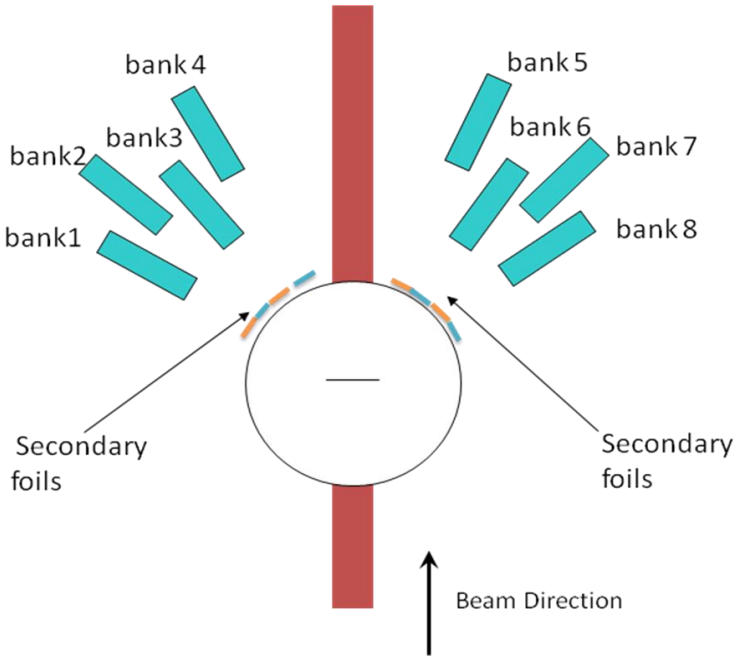

Figure 8 shows the detector and foil geometry B. The positions of the 4 secondary foils are shown as gold in "position 0" and blue for "position 1". **I**

In position 0. the foils were in the position illustrated in gold and were "in" for banks 1,3, 5 and 7, but "out" for banks 2,4,6 and 8.

In position 1. the foils were moved horizontally to the position illustrated in blue so that they were in for banks 2,4,6 and 8 and "out for banks 1,3, 5 and 7.

Figure 9 shows a calculation of background and data for lead with foil geometry B. It can be seen by comparing Figures 6 and 9 that the residual background is much smaller than with foil geometry A.

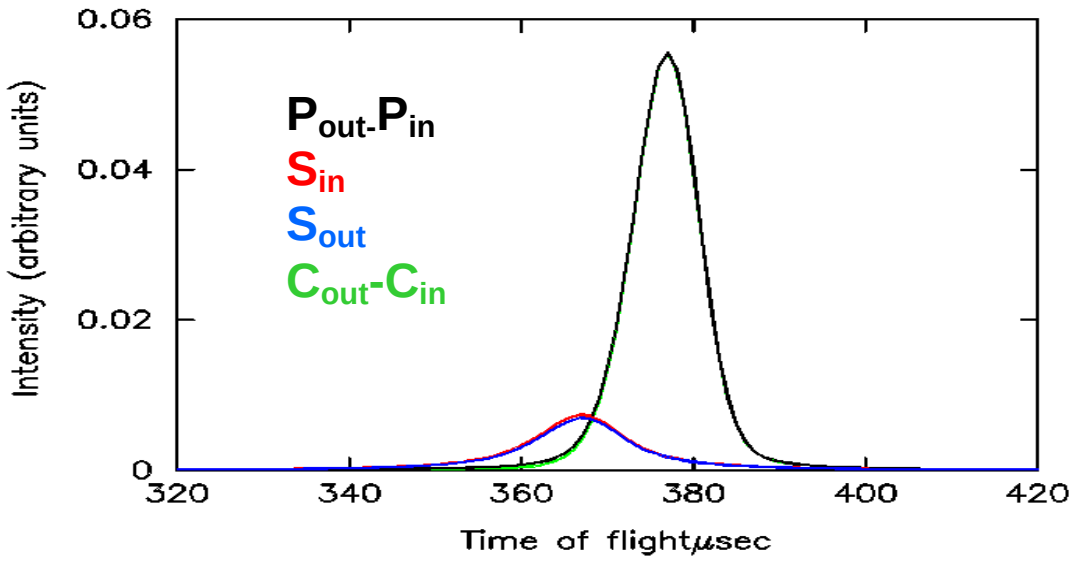

Figure 9. Calculation of background and data for lead in foil geometry B. Calculation was made for detector 1 in table 1 at a scattering angle of 66.6º and L_1=55cm.

Results for ZrH_2, are shown in Figure 10. The residual background is smaller than for foil geometry A, but is still significant. This is because (in contrast to foil geometry A) the

scattering angle θ_f of the secondary foils is different in the foil in and foil out measurements. Due to the anisotropy of the scattered neutron intensity from the hydrogen in the sample, the number of neutrons absorbed by the secondary foil is significantly different in the two foil positions. Hence the shape and intensity of the residual background changes in a complex way, determined by the geometry of the foils and detectors.

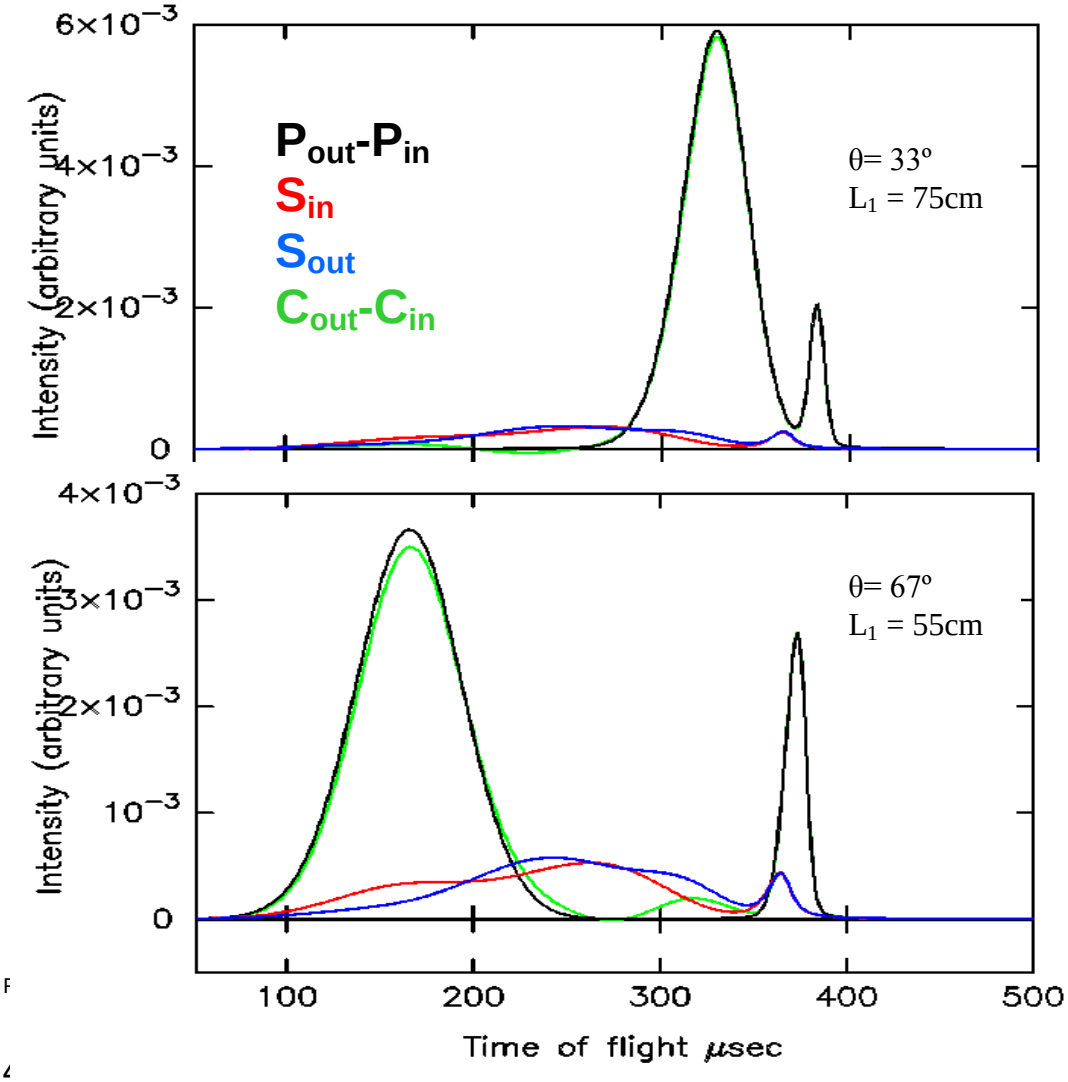

F

4

Foil Geometry A

We first compare the results of calculations and data with a lead sample. To increase statistical accuracy the data and calculations from the 8 "closest" detectors to the sample at ~56 cm (4,20,44,60,8,24,48,64 in table 1) were summed. A comparison was also made for the 8 detectors "furthest" from the sample (9,25,33,49,13,29,37,53 in table 1) at ~76 cm. The calculations were made for the values of scattering angle θ, final flight path L_1 and height h, determined for each detector by calibration [19]. The results are shown in Figure 11. The black line is the data. The red line is the calculation of $C_{out} - C_{in}$ given by eq (2.13) after

normalisation to the same area as the data. It can be seen that the calculation accurately reproduces the data.

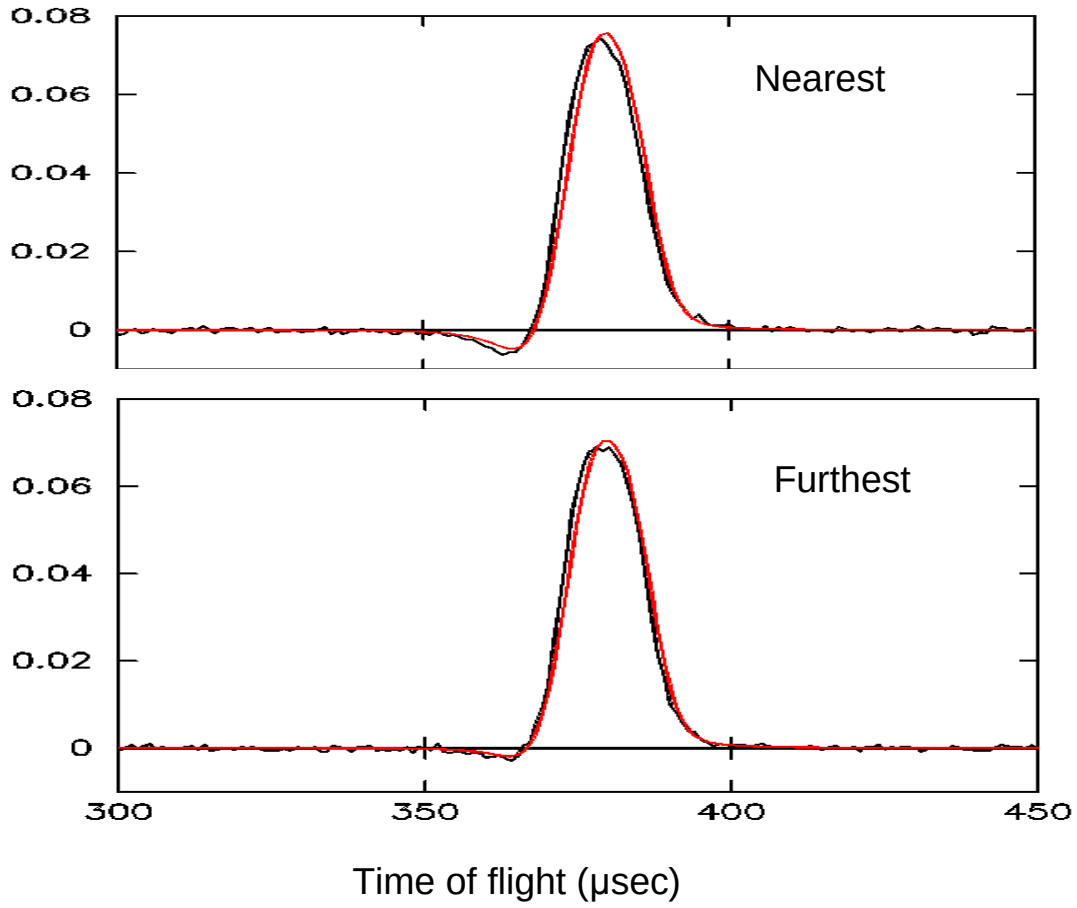

Figure 11. Data and calculation for the "nearest" and "furthest" detectors with a lead sample and foil geometry A. Data is in black, calculation in red.

The second comparison was made for a ZrH2 sample. To improve statistics the data from all detectors in a single bank at approximately the same scattering angle were summed. Again it is clear from Figure 12 that the calculation accurately reproduces the residual background from the secondary foils.

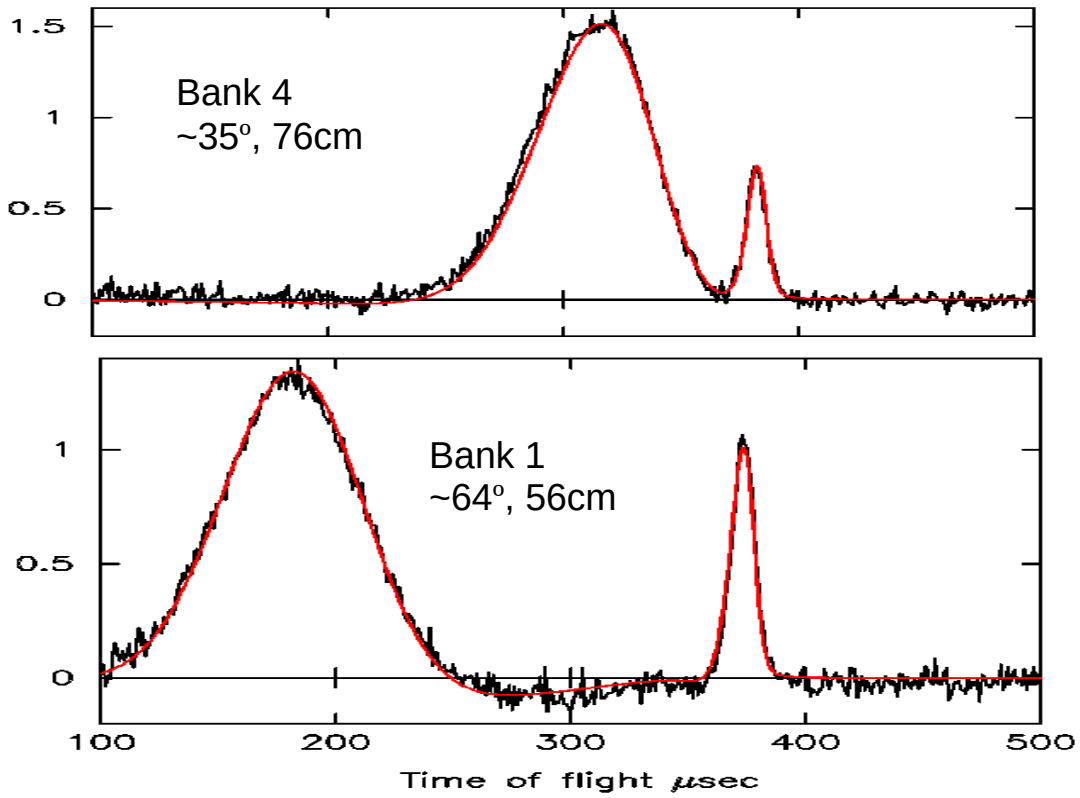

Figure 12 Shows data (black) and calculation (red) for ZrH2 from banks 1 and 4 in Foil geometry A . (runs 13344-13348)

Foil Geometry B

Figure 13 shows data (black) and calculation (red) for lead with foil geometry B. Figure 14 shows data and calculation for ZrH_2.

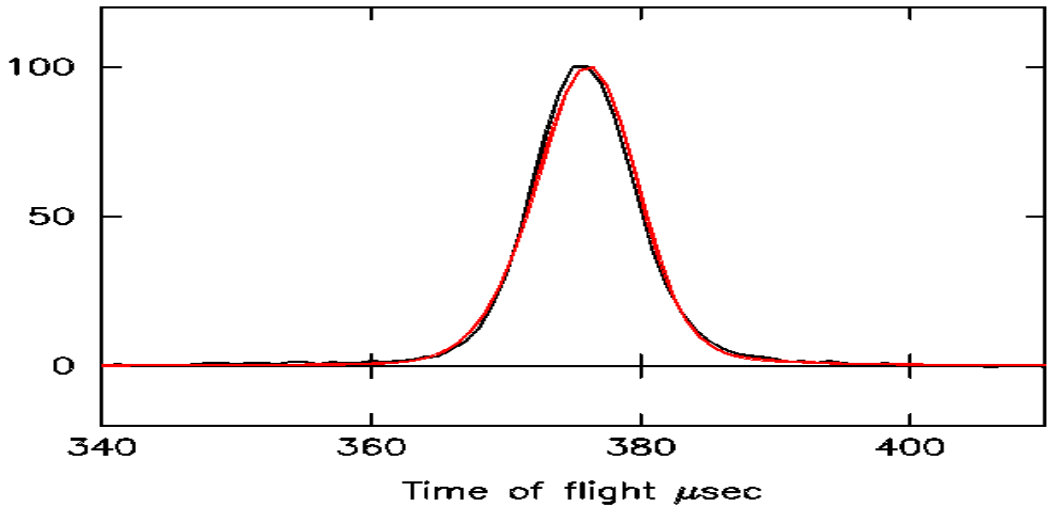

Figure 13.. Data and calculation on lead for foil geometry B, summed over detectors 1-8 in bank 4. The scattering angle of detectors were in the range 61° < θ < 67° . The sample-detector distance L_1 is ~76cm. Data and calculation for the "nearest" detectors with a lead sample and foil geometry A. Data is in black, calculation in red.

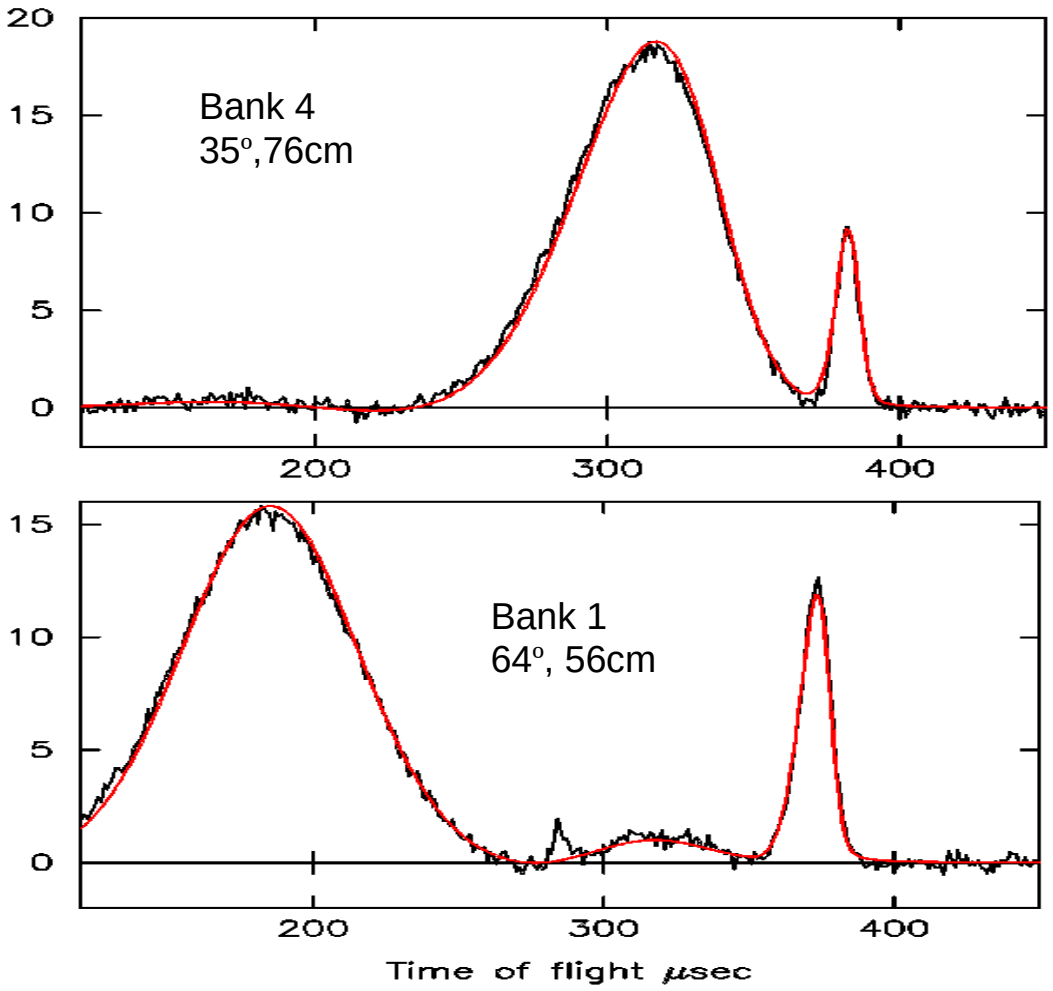

Figure 14. Data and calculated data from ZrH_2 from banks 4 and 1 with Foil geometry B . The sharp peak in the data at ~290 μsec is due to hafnium impurities.

5. Correction of data.

It is clear from Figures 11-14 that in all cases the residual background is reproduced well by the calculation. The calculation can therefore be used to correct the data for residual background. The procedure is as follows;

(1) Determine the function $C(E_0, E_1, \theta)$ from the uncorrected data (see Appendix 1).

(2) Calculate $P_{out} - P_{in}$, S_{out}, S_{in} and $C_{out} - C_{in}$ from eqs. (2.6),(2.7), (2.12) and (2.13)

(3) Calculate the normalisation factor F as

$$F = \frac{\int C_m(t)dt}{\int [C_{out}(t) - C_{in}(t)]dt} \qquad (4.4)$$

where $C_m(t)$ is the measured data and the integration is over the range of t analysed.

(6) Calculate the corrected data as

$$C_C = C_m - F(S_{out} - S_{in}) \qquad (4.5)$$

If necessary this procedure can be iterated. That is redetermine $C(E_0, E_1, \theta)$ from the corrected data and then recalculate the background correction. Empirically it is found that iteration makes little difference at the current levels of background on VESUVIO.
The efficiency with which neutrons are detected in the primary foil is determined by eq (2.4) and is uncertain to within a constant α

$$\eta = \tfrac{1}{2}\alpha\mu d \qquad (2.4)$$

This constant was determined by least squares fitting to ZrH2 data in the 48 YAP detectors and was found to be unity within error.

Examples of corrected and uncorrected data with foil geometry A and $\alpha = 1$ are shown in Figure 15 for lead and Figure 16 for ZrH_2. Figures 17 and 18 show the corresponding results for foil geometry B.

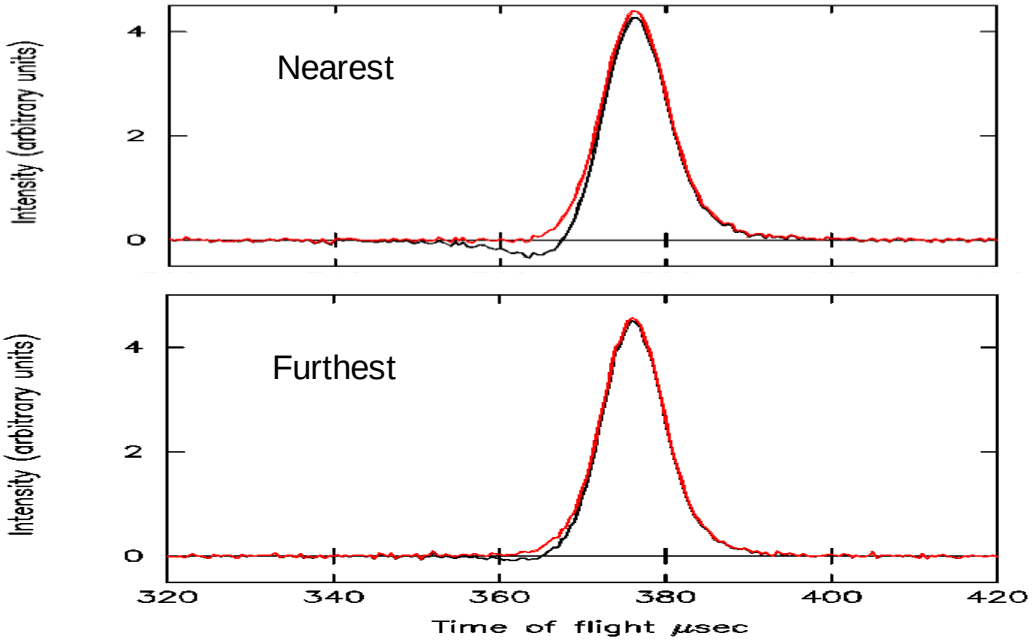

Figure 15. Lead data from the "nearest" and "furthest detectors" with foil geometry A. Black is uncorrected data. Red is corrected data

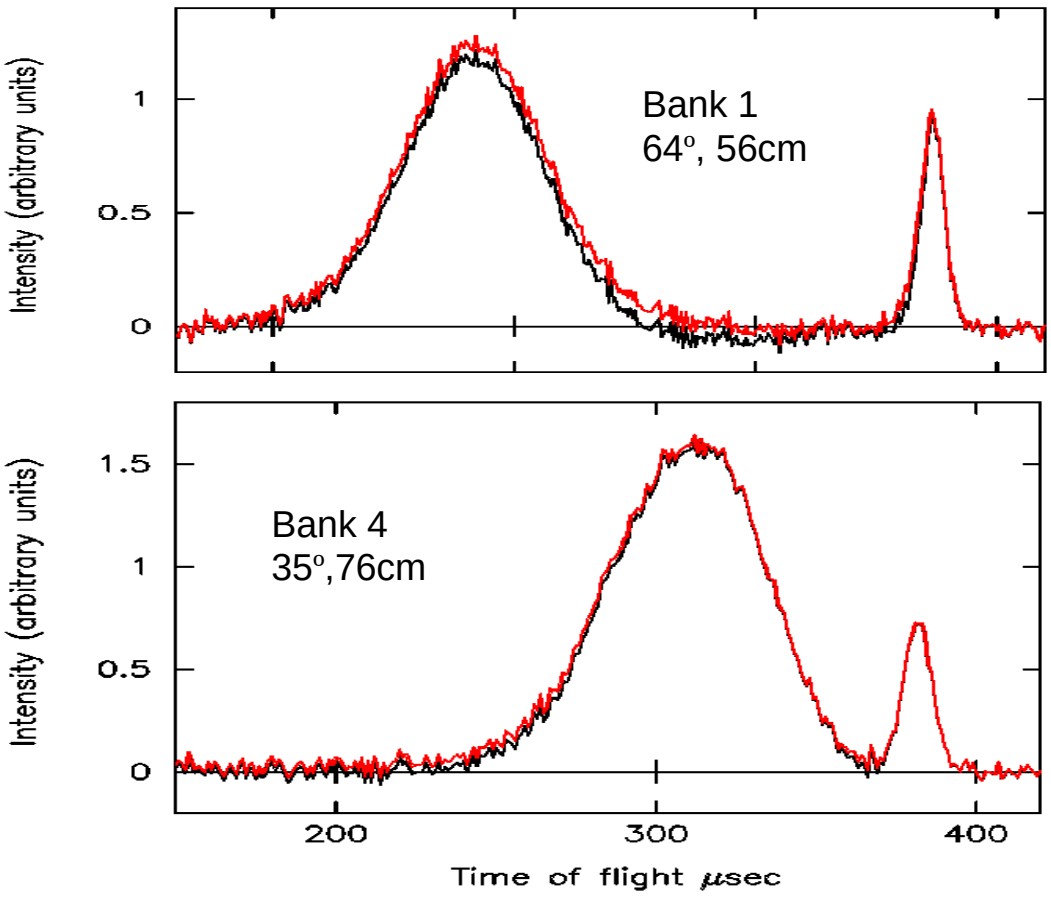

Figure 16. ZrH2 data from banks 4 and 1 with foil geometry A. Black is uncorrected data. Red is corrected data.

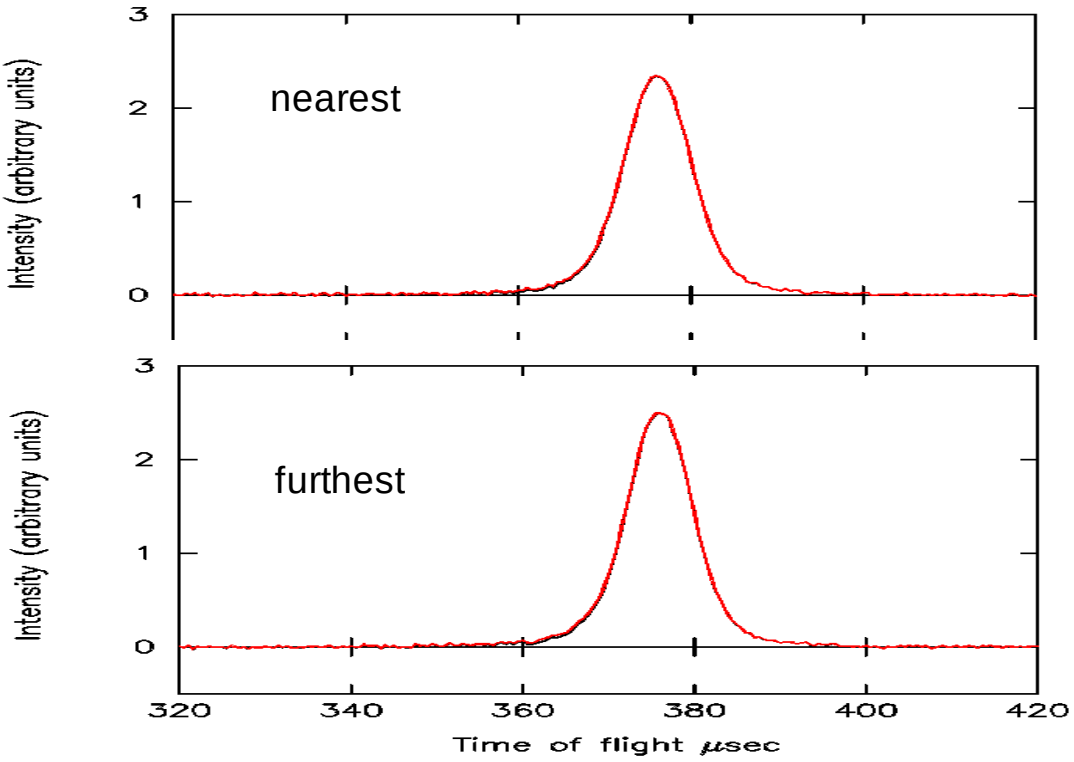

Figure 17. Sum of lead data from "nearest" and "furthest" detectors with foil geometry B. Black is uncorrected data. Red is corrected data

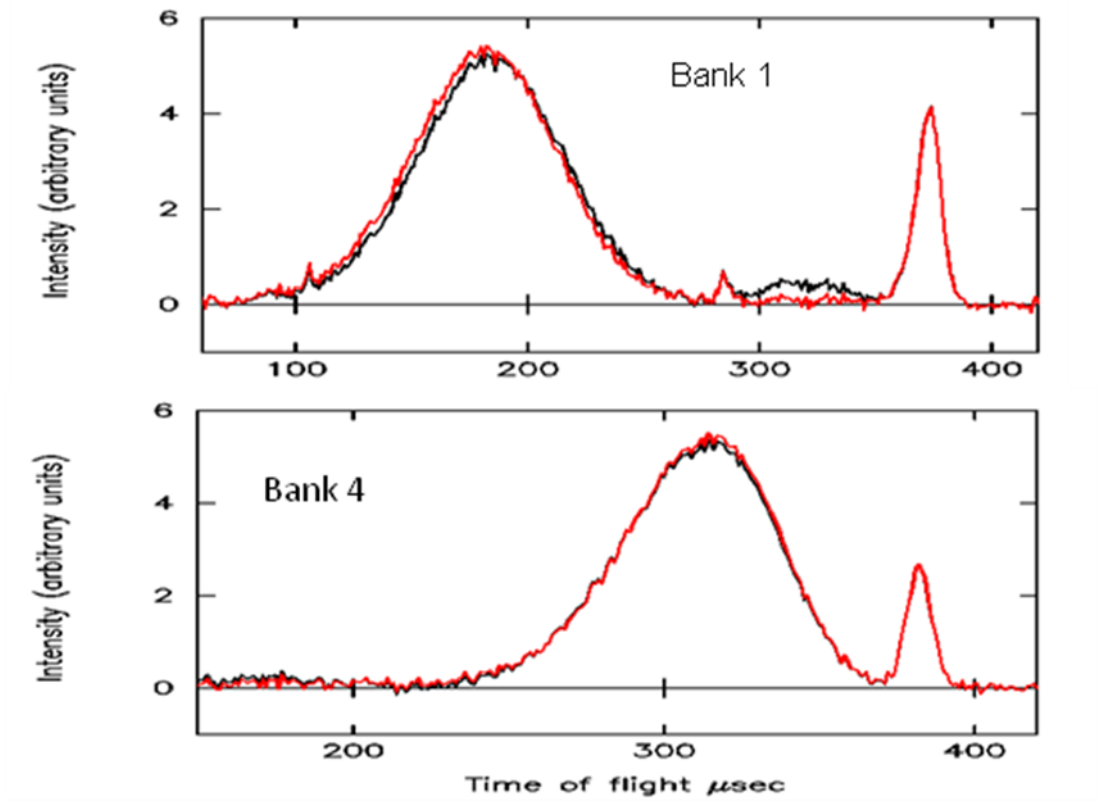

Figure 18. ZrH2 data from banks 1 and 4 with foil geometry B. Black is uncorrected data. Red is corrected data. The non-zero base .line at short times in Bank 4 is due to multiple scattering. The sharp peak at ~290 μsec is due to hafnium impurities in the ZrH2 sample used in this measurement.

6. Effects of γ-ray background on the results of data analysis

Results are presented for secondary foil geometry B, which is currently used on VESUVIO.

5.1 Amplitudes and widths.

The simplest method of data analysis on VESUVIO is to assume that all atoms of mass M have the same isotropic Gaussian momentum distribution with standard deviation w_M. The data can then be described with two fitting parameters for each atomic mass present; the mean momentum w_M and the overall intensity of scattering A_M. More detail is given in Appendix 1 and reference [10].

Figure 19a shows results of such an analysis on a sample of ZrH_2 contained in an aluminium can. The data shown is the sum of calibration runs performed between September 2008 and November 2009 with a total of ~27000 μamp-hours of beam. There are three masses present in the data; (1) hydrogen M =1.0079, (2) Zirconium, M =91, (3) Aluminium M =27. The ratio

$$R_H = A_1 / \sum_{n=1}^{3} A_n \qquad (5.1)$$

is the fraction of the total scattering which occurs from hydrogen atoms. R_H is shown for each detector in Figure 19a, with (black points) and without (red points) a correction for the residual background. The mean over the 64 detectors was 0.9305(4) before correction and

0.9301(4) after correction. The error is the standard error in the mean. It is clear that the gamma background has no significant effect on the measured hydrogen peak area. This has important implications since it implies that gamma background cannot explain the anomalous cross-section ratios measured on VESUVIO [10].

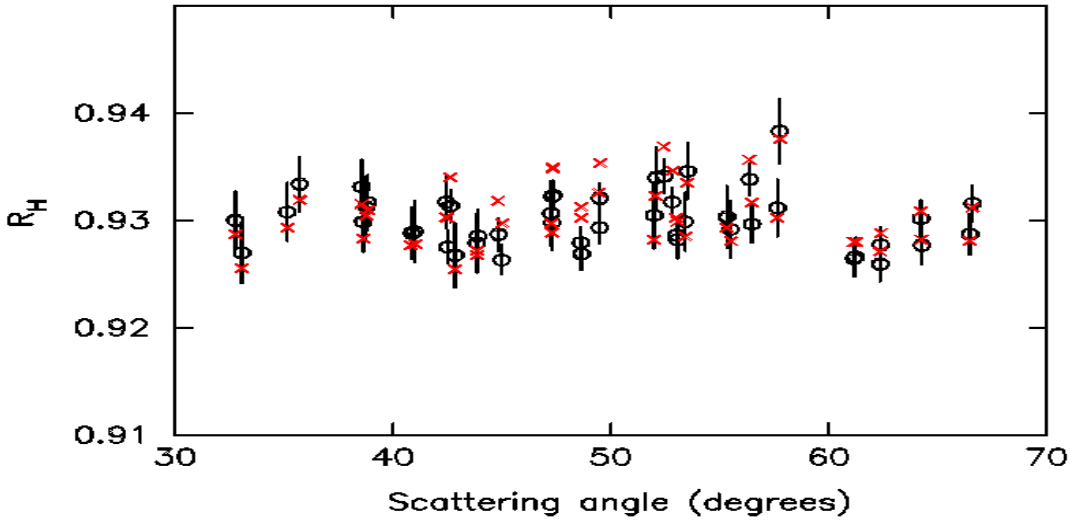

Figure 19a. Values of R_H for the 64 YAP detectors. The red points were obtained before correction for gamma background and the black points after correction. The statistical error on the red points is the same as that on the black points. The mean value of R_H before correction is 0.9305 (4) and after correction 0.9301(4).

Figure 19b shows corresponding values of w_M . Without a background correction the average of detectors 1-48 was w_M = 4.28 ±0.02 Å^{-1}, where the error is the standard error in the mean. With a correction for the gamma background this was reduced by ~2% to 4.14±0.01 Å^{-1}. The scatter on the points is also significantly reduced as reflected in the smaller standard error in the mean. This should be compared with the value for w_M of 4.16 Å^{-1} obtained from a harmonic calculation with the measured ZrH_2 density of states as input [22].

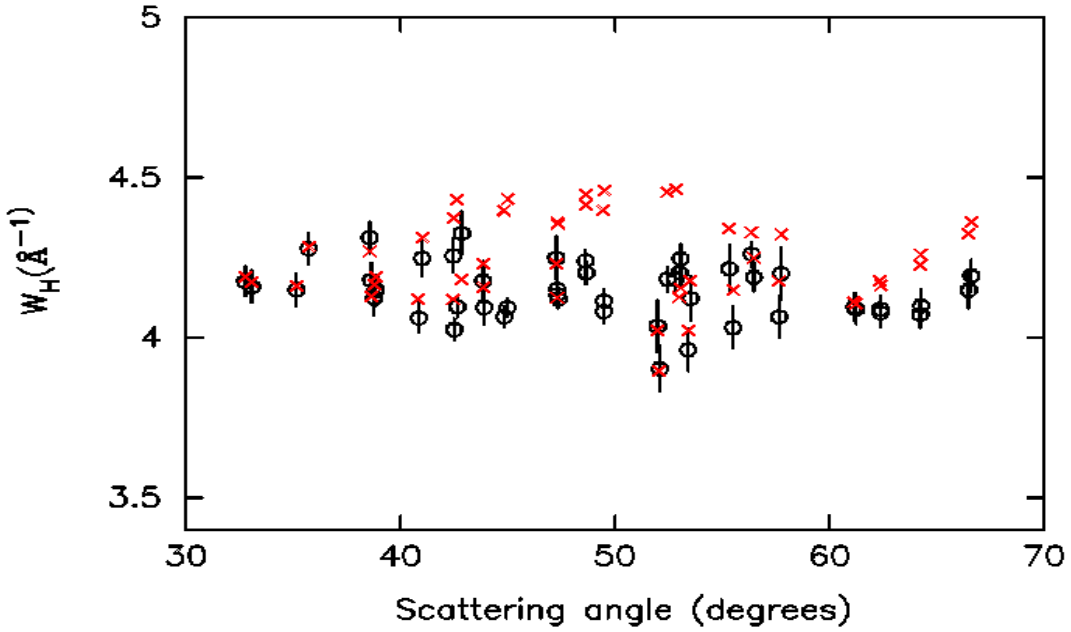

Figure 19b. Values of w_H in ZrH_2 for the 64 YAP detectors. The red points were obtained before correction for gamma background and the black points after correction. The widths are in $Å^{-1}$ and can be converted to momentum by multiplication by $\hbar$. The mean value of w_H before correction is 4.28 (2). The mean value after correction is 4.14 (1). The error quoted is the standard error in the mean

5.2 Effects on the shape of n(p).

In a more sophisticated analysis the momentum distribution for the protons is represented as the expansion given in equation (A1.14) This allows the shape of the proton momentum distribution to be determined in terms of the fitting parameters σ and c_n. The parameters c_n which are fitted are determined automatically using a routine based on the Bayesian methods described in references [23]. Typically 1-3 coefficients c_n are required to fit data on samples with no preferred direction - for example liquids and powders. The Bayesian routines find that for ZrH_2 only the c_2 parameter is significant for both corrected and uncorrected data.

Figure 20 shows the momentum distribution of the protons derived by simultaneously fitting the coefficients σ and c_2 to the data from detectors 1-48. The data is plotted as $p^2n(p)$ to emphasise the high values of p. $p^2n(p)$ obtained from fitting uncorrected data is shown in red, that from corrected in black.

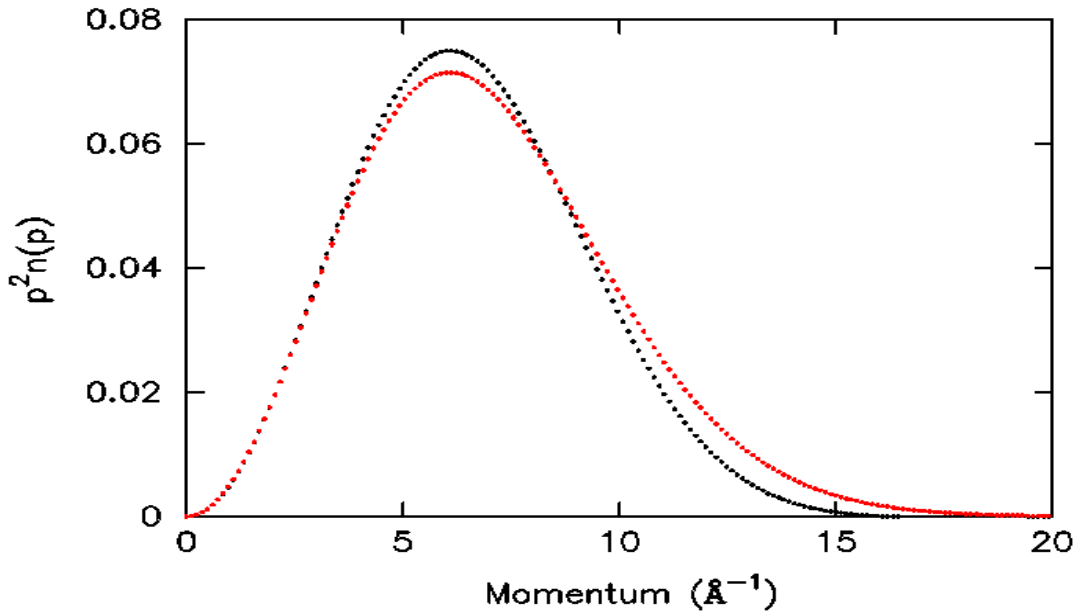

Figure 20. Shows $p^2n(p)$ without a background correction (red) and with a background correction (black). The error bars on the points are also shown.

As was the case with Gaussian fitting to the proton momentum distribution, the background in the current instrument configuration broadens the measured n(p).

7. Reduction of Residual background.

Although the residual gamma background can be calculated, it is clearly desirable to reduce it to as small a level as possible. There are a number of ways in which this can be done.

(a) Position the secondary foil closer to the sample. The number of γ-rays emitted by the secondary foil depends only upon the solid angle it subtends at the sample and is almost independent of its distance r_f from the sample. However the intensity of γ-rays from the secondary foil incident on the detector is proportional to $1/r_{fd}^{\ 2}$ where $r_{fd} \sim r_d - r_f$ is the distance from secondary foil to detector. The signal from the primary foils decreases as $1/r_d^{\ 2}$. Hence the signal to background ratio defined in eq (2.14) varies approximately as

$$S/C = (1 - r_f / r_d)^2 \qquad (6.1)$$

The constant C depends upon the precise instrument geometry used. The function S/C is shown in Figure 21.

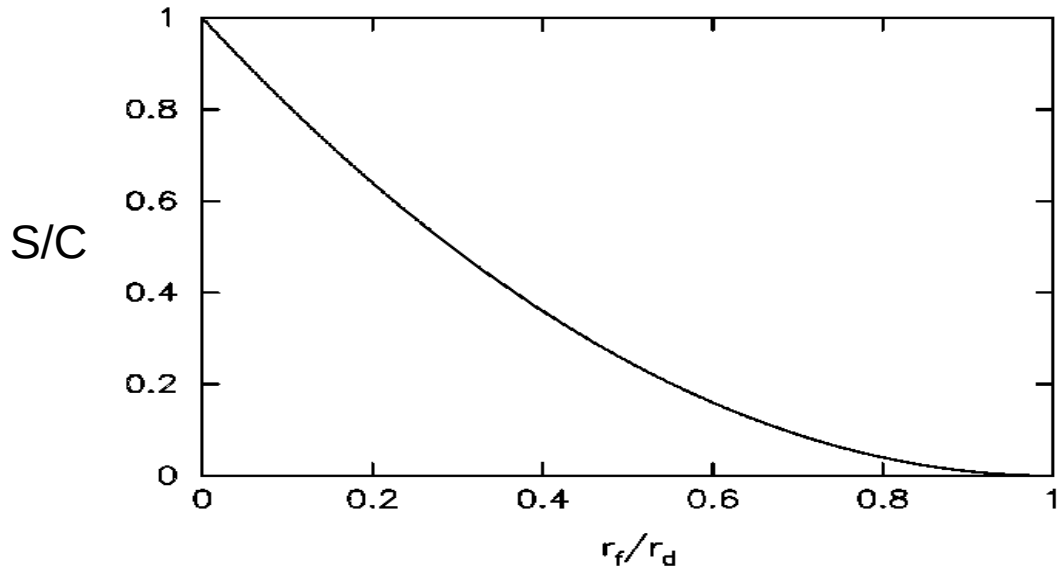

Figure 21. Shows the function S/C defined in eq. 6.1 as a function of the ratio r_f / r_d, where r_f is the distance to the secondary foil and r_d that to the detector.

(b) Move the detectors further from the sample. This allows the ratio r_f / r_d to be reduced. For example with the current VESUVIO geometry r_f =22.5 cm; for the detectors at r_d = 56cm, r_f / r_d ~0.4 and S/C = 0.36 while for the detectors at 76 cm r_f / r_d ~0.3 and S/C =0.49 Moving the detectors to 200cm would increase S/C to 0.76 giving almost a factor of two decrease in the residual background compared with 56cm.

(c) Ensure that the secondary foils move as little as possible between the foil in and foil out positions. The smaller movement of the secondary foils with foil geometry B is primarily responsible for the reduction in residual background compared with geometry A.

(d) Keep the scattering angle to the secondary foils the same in the two positions. This is important mainly for measurements on protons and to a lesser extent on deuterons.
For example although it can be seen from Figures 6 and 9 that foil geometry B is much better for heavy atoms such as lead, the improvement is not so great for hydrogen atoms. In the latter case the intensity of scattered neutrons incident on the secondary foils depends strongly on the angle θ_f (see Figure 4). If θ_f is different in the two foil positions the residual background is still significant. (see Figures 7 and 10).

A preferable secondary foil and detector geometry would be with all detectors and foils on rings. By rotation of the ring containing the secondary foils, strips of foil could be moved between foil in and foil out positions, while remaining at the same scattering angle.

8. Summary and Conclusions

It has been shown that the replacement of the VESUVIO forward scattering bank by YAP γ-ray detectors has lead to a significant improvement in the instrument resolution. However it has also lead to a sample dependent background. Without data correction the residual background leads to no significant change in the measured intensity of the hydrogen signal but a ~ 2% increase in the measured width. It has been shown that the residual background can be calculated from the data and that accurate data correction can be incorporated in the data-analysis software. Ways in which the residual background could be reduced have been discussed.

Appendix 1. Data analysis on VESUVIO.

The count rate at time of flight t in an inverse geometry spectrometer (that is one where the energy of the scattered neutron is fixed) is [24]

$$C(t) = 2\left(\frac{2}{m}\right)^{1/2} \frac{E_0^{3/2}}{L_0} I(E_0) D(E_1) N \frac{d^2\sigma}{d\Omega dE_1} d\Omega \qquad \text{(A1.1)}$$

m is the neutron mass, L_0 the incident flight path, $I(E_0)$ is the intensity of incident neutrons of energy E_0 , $D(E_1)$ is the probability that scattered neutrons of energy E_1 are detected, N is the number of atoms in the beam, $d^2\sigma/d\Omega dE_1$ is the average partial differential scattering cross-section of an atom and $d\Omega$ is the solid angle subtended by the detector (see Figure A1).

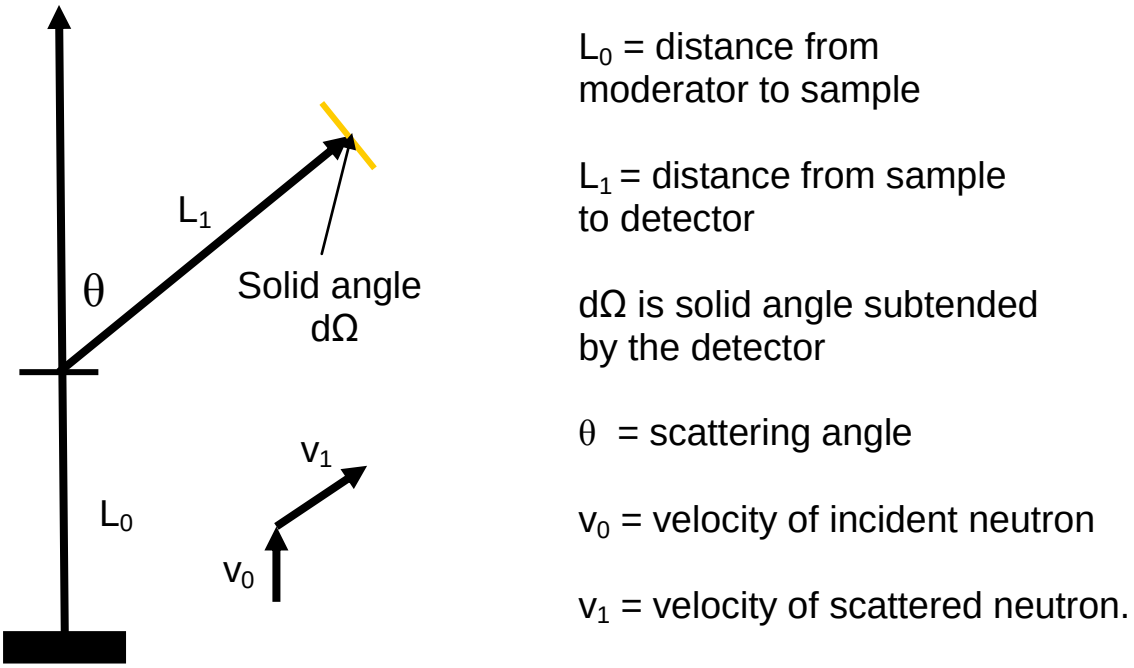

Figure A1. Illustrates a time of flight measurement on VESUVIO.

The energy transferred from neutron to sample is

$$\omega = E_0 - E_1 \tag{A1.2}$$

and the momentum transfer is

$$q = \sqrt{2m}\left(E_0 + E_1 - 2\sqrt{E_0 E_1}\cos\theta\right)^{1/2} \tag{A1.3}$$

The measured time of flight of the neutron is

$$t = \frac{L_0}{v_0} + \frac{L_1}{v_1} + t_0 \tag{A1.4}$$

where

$$v_0 = \sqrt{2E_0/m} \qquad v_1 = \sqrt{2E_1/m} \tag{A1.5}$$

L_0 is the incident flight path L_1 is the sample-detector distance, t_0 is the time at which neutrons leave the source. Since v_1 is defined by the energy of the gold foil absorption resonance, v_0 can be determined from eq. (A1.4). Hence ω and q can be determined from eqs (A1.2) and (A1.3) for each time of flight value t.

The basic assumption of VESUVIO data analysis is that the impulse approximation (IA) is accurate. The validity of the IA in neutron scattering has been discussed by many authors [25,26,27, 28]. At the energy and momentum transfers attained on VESUVIO the IA is accurate to within ~5% in hydrogenous samples.[29]. Deviations from the IA are also well understood and can be accurately calculated. After correction residual inaccuracies due to breakdown of the IA are less than 0.3%.

A basic assumption of the IA is that the scattering is incoherent - that is the sum of scattering from the individual atoms. Thus if atoms of different mass M are present in the sample

$$N\frac{d^2\sigma}{d\Omega dE_1} = \sum_M N_M \frac{d^2\sigma_M}{d\Omega dE_1} d\Omega \tag{A1.6}$$

where N_M is the number of atoms and $d^2\sigma_M / d\Omega dE_1$ is the partial differential cross-section for mass M.

$$\frac{d^2\sigma_M}{d\Omega dE_1} = |b_M|^2 \sqrt{\frac{E_1}{E_0}} S_M(\mathbf{q},\omega) \tag{A1.7}$$

where b_M is the bound neutron scattering length of atoms of mass M and $S_M(\mathbf{q},\omega)$ is the incoherent dynamic structure factor [9].

According to the IA

$$S_M(\mathbf{q},\omega) = \int n_M(\mathbf{p})\delta\left(\omega + \frac{p^2}{2M} - \frac{(\mathbf{p}+\mathbf{q})^2}{2M}\right) d\mathbf{p} \tag{A1.8}$$

where $n_M(\mathbf{p})$ is the atomic momentum distribution for mass M [9]. The physical content of eq. (A1.9) is that the IA treats the scattering as single atom "billiard ball" scattering with conservation of momentum and kinetic energy of the neutron + target atom.

It follows from (A1.8) that

$$S_M(\mathbf{q},\omega) = \frac{M}{q} J_M(y_M, \hat{\mathbf{q}}) \tag{A1.9}$$

where

$$y_M = \frac{M}{q}\left(\omega - \frac{q^2}{2M}\right). \tag{A1.10}$$

$$J_M(y_M, \hat{\mathbf{q}}) = \int n_M(\mathbf{p})\delta(y_M - \mathbf{p}\cdot\hat{\mathbf{q}})d\vec{p} \tag{A1.11}$$

and $\hat{\mathbf{q}}$ is the unit vector along $\mathbf{q}$. For atoms bound by isotropic harmonic forces $J_M(y_M, \hat{\mathbf{q}})$ is the same for all directions $\hat{\mathbf{q}}$ and (A1.11) reduces to a normalised Gaussian function [9].

$$J_M(y_M) = \frac{1}{\sqrt{2\pi w_M{}^2}} \exp\left(\frac{-y_M{}^2}{2w_M{}^2}\right) \tag{A1.12}$$

The simplest method of data analysis is to assume that $J_M(y_M)$ for all atoms has the form given in eq (A1.12). The data can then be described with two fitting parameters for each atomic mass present; the mean atomic momentum w_M and $A_M = N_M b_M{}^2$. More details of this procedure are given in reference [10]. Once w_M and A_M for each mass have been determined by fitting the data, the function $C(t)$ in eq (A1.1) is determined to within a constant factor from eqs (A1.2) - (A1.12),.

Comparing eqs (1.1) and (A1.1),

$$C(E_0, E_1, \theta) = 2\left(\frac{2}{m}\right)^{1/2} \frac{E_0{}^{3/2}}{L_0} I(E_0) N \frac{d^2\sigma}{d\Omega dE_1} d\Omega \tag{A1.13}$$

Hence the fit to the data can be used to determine $C(E_0, E_1, \theta)$. The residual background van then be calculated via the algorithm in section 2.

Anharmonicity and anisotropic binding forces lead to non-Gaussian behaviour. This can be measured by representing the neutron Compton profile of a particular mass as

$$J(y) = \frac{1}{\sqrt{2\pi\sigma^2}} \exp\left(\frac{-y_M{}^2}{2\sigma^2}\right) \sum_n \frac{c_n}{2^n n!} H_{2n}\left(\frac{y}{\sqrt{2}\sigma}\right) \tag{A1.14}$$

Where H_n are Hermite polynomials and σ, c_n are fitting parameters. In principle any form of $J(y)$ can be represented by this expansion which is complete. In practice 1-4 parameters c_n are required to fit data from powders and liquids. Given the fitted coefficients σ, c_n, the momentum distribution $n(p)$ is given by [30]

$$n(p) = \frac{1}{(2\pi\sigma^2)^{3/2}} \exp\left(\frac{-p^2}{2\sigma^2}\right) \sum_n c_n (-1)^n L_n^{1/2}\left(\frac{p}{\sqrt{2}\sigma}\right) \qquad \text{(A1.15)}$$

Where $L_n^{1/2}$ are generalised Laguerre polynomials.

Appendix 2 Calculation of the count rate from the primary foil.

The count rate in the YAP detectors depends upon the efficiency with which γ-rays emitted when the foil absorbs a neutron are detected. This depends upon the energy and direction of emission of the γ-rays. We take coordinate axes with z perpendicular to the detector surface, y along the length of the detector and x along the width as shown in Figure A2.1. γ-rays are emitted from a gold foil of negligible thickness on the surface of the detector, which is taken as the plane $z = 0$.

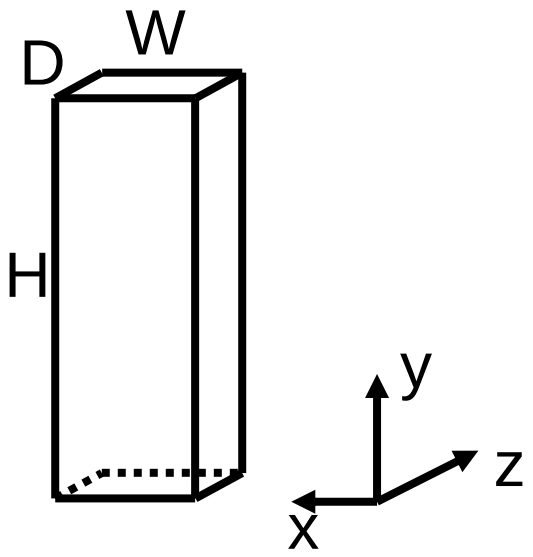

Figure A2.1. Illustrates a detector of width W, height H and thickness D. The orientation of the coordinate system is also shown.

Consider a γ-ray emitted from the point $\mathbf{r}_p = (x_p, y_p, 0)$, with $0 < x_p < W$, $0 < y_p < H$, and parallel to the unit vector

$$\hat{\mathbf{n}} = \sin\theta\cos\phi\hat{\mathbf{x}} + \sin\theta\sin\phi\hat{\mathbf{y}} + \cos\theta\hat{\mathbf{z}} \qquad \text{(A2.1)}$$

The equation of the line of travel of the γ-ray is

$$\mathbf{r} = \mathbf{r}_p + \alpha\hat{\mathbf{n}} \qquad \text{(A2.2)}$$

That is

$$x = x_p + \alpha \sin\theta\cos\phi \qquad \text{(A2.3)}$$

$$y = y_p + \alpha \sin\theta\sin\phi$$

$$z = z_p + \alpha\cos\theta$$

The γ-ray intersects the planes containing the scintillator glass at the following positions;

$x = 0$ when $\alpha_1 = \dfrac{-x_p}{\sin\theta\cos\phi}$, $\qquad x = W$ when $\alpha_2 = \dfrac{W - x_p}{\sin\theta\cos\phi}$ (A2.4)

$y = 0$ when $\alpha_3 = \dfrac{-y_p}{\sin\theta\sin\phi}$, $\qquad y = H$ when $\alpha_4 = \dfrac{H - y_p}{\sin\theta\sin\phi}$ (A2.5)

$z = 0$ when $\alpha_6 = (-z_p)/\cos\theta$ $\qquad z = d$ when $\alpha_6 = (d - z_p)/\cos\theta$. (A2.6)

The distance along the line from the point $\mathbf{r}_p = (x_p, y_p, 0)$ is α. Negative α_i corresponds to a γ-ray emitted in the opposite direction to the glass. The distance l travelled by a γ-ray emitted towards the glass is therefore the minimum of the positive values of α_i.

The algorithm used to calculate the probability that a γ-ray ray emitted by the primary foil is detected is as follows;

1. Randomly generate x_p according to the uniform distribution 0<x<W

2. Randomly generate y_p according to the uniform distribution 0<y<L

3. Randomly generate θ according to the uniform distribution $0 < \theta < \pi/2$ and weight by $\frac{1}{2}\sin\theta d\vartheta$. This is the probability that γ-rays emitted isotropically will be at an angle θ to the z axis.

4. Generate ϕ according to the uniform distribution $0 < \phi < 2\pi$.

5. Calculate $\alpha_1, \alpha_2, \alpha_3, \alpha_4, \alpha_5, \alpha_6$ from eqs. (2.4)-(2.6).

6. Determine the distance l travelled by the γ-ray in the scintillator glass as the smallest of the positive values of the α_i

(7) Calculate the probability of absorption as $1 - \exp(-\mu t)$.

(8) Calculate the total probability of this event as

$$P_{ab} = \tfrac{1}{2}\sin\theta\left[1 - \exp(-\mu l)\right] \approx \tfrac{1}{2}\mu l \sin\theta. \qquad \text{(A2.7)}$$

In order to determine the average probability $\overline{P_{ab}}$ of absorption a large number of events are generated using a random number generator and the average calculated. $\overline{P_{ab}} / \mu d$ is shown

as a function of μD in Figure A2.2. $\overline{P_{ab}}$ increases at low values of μD where it is dominated by γ-rays emitted close to the plane of the scintillator glass.

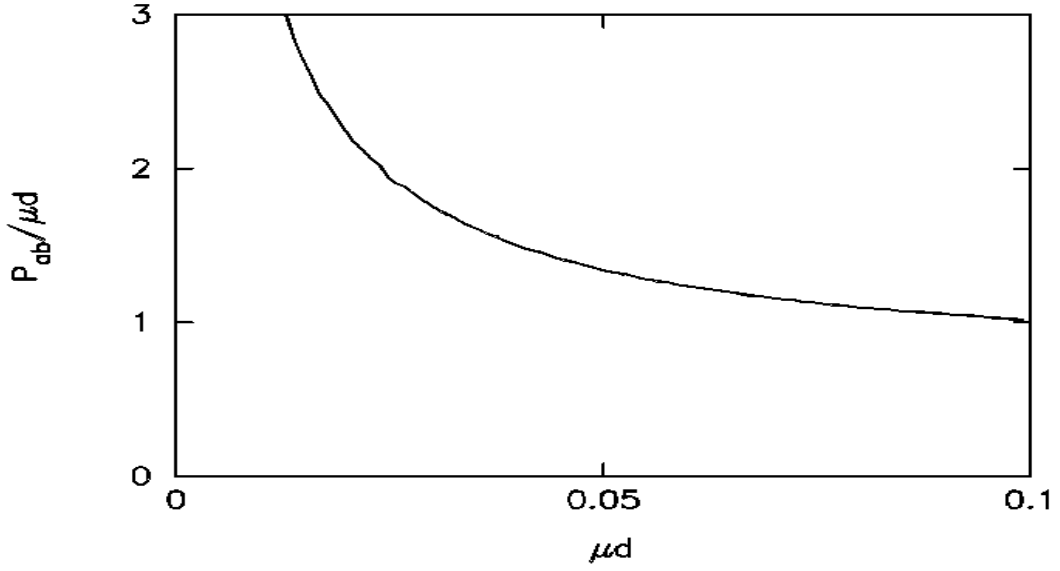

Figure A2.2. Shows calculated values of $\overline{P_{ab}} / \mu d$ as a function of μd . Calculated using [.yap]pcount.for.

Since $\overline{P_{ab}}$ is the probability that γ-rays emitted toward the detector are registered, the probability that γ-rays emitted isotropically by the primary foil are detected is $\frac{1}{2}\overline{P_{ab}}$. It follows that

$$\alpha = \overline{P_{ab}} / \mu d \qquad \text{(A2.8)}$$

Appendix 3. Programs used to calculate and correct for background

Bcalc.for

This calculates data and γ-ray background for the original foil arrangement on VESUVIO which was in place for runs 12572-13348

Input is; (a) .in file such as zh_bcalc.in

0001	! Ipno
4908 24.0 74.0	! E1, DE1L,DE1G
3	! Number of masses
1.0079 0.931 4.19	! First mass, intensity,width
27.0 0.038 14.7	! 2cnd mass, intensity,width
91.0 0.031 23.0	! 3rd mass, intensity,width
0	! Option for MS 0 gives no MS
[evsmgr.jm.ms]zh2572	! Name of file containing calculated MS.

(b) Detector position read in from [.YAP]DETPOS.DAT. This contains the detector positions in cylindrical co-ordinates rho,phi,z.

The output is in files CDET_1.dat .. CDET_64.dat. These files are normalised so that the total area is 1. These can be read into GENIE using the >FILEREAD command.

BCALCW.FOR

This is identical to BCALC but also outputs;
Total cts unnormalised.
Cts with no background into files CDETNB_1.dat etc,
the secondary counts with the foils in the up position into cdetup_1.DAT ETC,
the secondary counts with the foils in the down position into CDETDOWN_1.dat etc.
The residual background into BACK_1.dat etc.
This program was used to generate the plots shown in Figures 7 and 8.

Bcorr.for

This has identical input to BCALC.FOR. It subtracts the residual background according to the algorithm given in section 2 for the original foil arrangement on VESUVIO which was in place for runs 12572-13348. It works correctly for data simulated by BCALC2.

Bcalc2.for

This is identical to Bcalc.for, but calculates for the second foil arrangement now in place on VESUVIO. That is for run numbers greater than 13348. The γ-ray background for detectors 49-64 is multiplied by a factor 2 to allow for the incomplete coverage of these detectors by the secondary foil

Bcalc2W.for

This is identical to Bcalcw.for, but calculates for the second foil arrangement now in place on VESUVIO. That is for run number greater than 13348.
CDET_1.dat etc contain the data with residual background
CTD_1.DAT etc contain the data with no background.
CT0_1.DAT etc contain the background from secondary foils in position 0.
CT1_1.dat etc contain the background from the secondary foils in position 1.
BACK_1.dat etc contains the residual background. For detectors 9-16,49_56 and 57-64 this is multiplied by 2.
The γ-ray background for detectors 49-64 is multiplied by a factor 2 to allow for the incomplete coverage of these detectors by the secondary foil

This program was used to generate Figures 11 and 12.

Bcorr2.for

This has identical input to BCORR2.FOR. It subtracts the residual background according to the algorithm given in section 2 for the second foil arrangement on VESUVIO which was in place for run number greater than13348. It works correctly for data simulated by BCALC2. The γ-ray background for detectors 49-64 is multiplied by a factor 2 to allow for the incomplete coverage of these detectors by the secondary foil

---

1 *Measurement of momentum distributions of light atoms and molecules in condensed matter systems using inelastic neutron scattering.* C Andreani, D Colognesi, J Mayers and G Reiter. Adv Phys **54** 377-469 (2005)

2 *Excess of proton mean kinetic energy in supercooled water.* A Pietropaolo, R Senesi, C Andreani et al. *Phys. Rev. Lett.* ***100*** *127802 (2008).*

3 *Proton momentum distribution in liquid water from room temperature to the supercritical phase.* C. Pantalei, A. Pietropaolo, R. Senesi, S. Imberti, C. Andreani, J. Mayers, C. Burnham, and G. Reiter. *Phys. Rev. Lett.* ***100*** *177801 (2008)*

4 *Measurement of the kinetic energy and lattice constant in hcp solid helium at temperatures 0.07-0.4K.* M Adams and J Mayers *Phys. Rev. Lett.* ***98*** *85301(2007).*

5 *Quantum and classical relaxation in the proton glass .* Y. Feng, C. Ancona-Torres et al. *Phys. Rev. Lett.* ***97*** *69901 (2006)*

6 *Anomalous behaviour of proton zero point motion in water confined in carbon nano-tubes.* G. Reiter, C. Burnham et al *Phys. Rev. Lett.* ***97*** *247801 (2006).*

7 *Proton momentum distribution in a protein hydration shell.* R. Senesi, A Pietropaolo et al. *Phys. Rev. Lett.* ***98*** *138102 (2007)*

8 *Measurement of the 3-D Born-Oppenheimer potential of a proton in a hydrogen-bonded system via deep inelastic neutron scattering.* D Homouz, G. Reiter et al. *Phys. Rev. Lett* ***98*** *115502 (2007)*

9 *Theory of Neutron Scattering from Condensed matter Volume 1*, S W Lovesey, (Oxford University Press 1984) sections 3.4,

10 *The measurement of anomalous neutron inelastic cross-sections at electronvolt energy transfers*. J Mayers and T Abdul-Redah, J. Phys. Condens. Matter 16 (2004) 4811–4832

11 *Pulsed Neutron Scattering*, C. Windsor, Taylor and Francis, London, (1981).

12 *Double Difference method to improve the resolution of an eV neutron spectrometer.* P.A. Seeger, A.D. Taylor and R. M. Brugger, *Nucl. Instr. Methods* **A 240**, 98 (1985).

13 *Advances on detectors for low-angle scattering of epithermal neutrons* E P Cippo, G Gorini, M Tardocchi, et al. Measurement Science and Technology **19** 47001 (2008)

14 *YAP Scintillators for resonant detection of epithermal neutrons at pulse neutron sources.* M. Tardocchi, G. Gorini et al. *Rev. Sci. Inst.* **75,** 4880 (2004).

15 *A resonant detector for high-energy inelastic neutron scattering experiments.* C. Andreani, A. Pietropaolo et al. Applied Physics Letters **85** 5454 (2004)

16 *Foil cycling technique for the VESUVIO spectrometer operating in the resonance detector configuration,* E M Schoonveld, J. Mayers et al Rev. Sci. Inst. **77** 95103 (2006)
Author(s): Schooneveld EM, Mayers J, Rhodes NJ, et al.

17 *Foil cycling technique for the VESUVIO spectrometer operating in the resonance detector configuration,* E M Schoonveld, J. Mayers et al Rev. Sci. Inst. **77** 95103 (2006)
Author(s): Schooneveld EM, Mayers J, Rhodes NJ, et al.

18 *Calibration of the electron volt spectrometer, a deep inelastic neutron scattering spectrometer at the ISIS pulsed neutron spallation source.* A. L. Fielding and J. Mayers, *Nucl. Inst. Meth. A*, **480**, 680 (2002).

19 *Calibration of the electron volt spectrometer VESUVIO at ISIS.* Rutherford-Appleton Laboratory technical report RAL-TR-2009-22

20 G Gorini, A. Pietropaolo, private communication.

21 *Neutron Cross Sections* ,S.F. Mughabghab, (Academic Press, Orlando, Florida, 1984).

22 *Neutron-scattering study of the impulse approximation in ZrH2*, A. C. Evans, D. N. Timms, J. Mayers and S. M. Bennington Phys Rev B 53 3023 (1996)

23 *Data Analysis. A Bayesian Tutorial*,D. Sivia (Clarendon Press Oxford 1996) Section 4.2

24 Ref [11] equation (9.30).

25 V. F. Sears *Phys. Rev. B.* **30,** 44 (1984).

26 J Mayers, C Andreani, G Baciocco, *Phys Rev B* **39** 2022 (1989)

27 J Mayers *Phys Rev B* **41,** 41 (1990)

28 See H R Glyde *Phys Rev B.* **50** 6726, (1994) for a recent review of the literature on FSE.

29. A.C. Evans, D.N. Timms, J. Mayers and S. Bennington, Phys Rev B **53** 3023 (1996).

30 G. F. Reiter, J. Mayers, and J. Noreland, Phys. Rev. B **65**, 104305 (2002).